The International Journal of Advanced Manufacturing Technology (2020) 107:689–704
https://doi.org/10.1007/s00170-019-04806-8

ORIGINAL ARTICLE

Peg-on-hole: mathematical investigation of motion of a peg and of forces of its interaction with a vertically fixed hole during their alignment with a three-point contact

Ludmila B. Chernyakhovskaya[1] · Dmitry A. Simakov[2]

Received: 16 July 2019 / Accepted: 9 December 2019 / Published online: 19 February 2020

Abstract
The task of the peg-in-hole assembly is a very common task in industry. Despite its intuitive comprehensibility and everyday experience, the industrial assembly faces specific problems. The naive approach of inserting with bare hands an industrial peg inside into an industrial hole can very certainly bring to the jamming and damaging because of a very small gap between them. Therefore, the initial alignment of the details before insertion, so-called peg-on-hole phase, or simply peg-on-hole, is of the special importance in industry to avoid jamming. This paper develops the description and analysis of this phase based on the methods of analytical mechanics. As a common approach, the details in this study are considered as cylindrical, and such that peg is supported at the edge of vertically fixed hole, and could freely move keeping a three-point contact with three degrees of freedom, namely (i) nutation angle or align describing planar motion of aligning parts, (ii) precession angle or slide describing rotational motion around hole axis, and (iii) self-rotation angle or slip describing rotational motion about its axis. The analytical approach implies the system of Lagrange Equations for this particular case of motion, which is called Dynamic Differential Equations (DDE). DDE describes interconnections between motion in three degrees of freedom on one side, reaction forces on another side, and the external forces and torques on the third side. DDE includes geometrical properties of the details, and full descriptions of velocities, normal reactions, and friction forces at the contact points. It is the most general description of the peg-on-hole case. As the example of application, the normal reactions were found for relative large alignment angles far from reduction into a two-point contact, and for a small alignment angles, when system transits to the two-point contact. It was shown that for both cases, reaction forces become larger during alignment because they have to balance the force of gravity. For the larger angles, slip reduces the reaction forces, whereas for small alignment angles, slip and slide increases them.

Keywords Cylindrical parts · Three contact points · Compound motion · Three degrees of freedom · Dynamic responses · Differential equations · Robotic assembly

1 Introduction

Assembly of cylindrical peg inside the hole, which is also called peg-in-hole, is of great importance. In machine-building industry, it may amount to about 20%, and in instrument-making industry—up to 40% of all assembly operations. Since the risk of jamming and damage requires special control during the operation, automation of the process is a relevant task, and robotic systems have increasingly been in use to cope with it.

The comprehensive overview of the investigations related to the peg-in-hole insertion was done by [1] and the latest in 2019 by [2] including the most up-to-date results for peg-in-hole studies. The investigations involve the strategies that could be largely divided into contact model–based and contact model–free control systems. The contact model–based strategies tend to either recognize the contact state [3–5] or control of compliance of assembly [6–8]. The contact model–free include learning from the demonstration like a human hand [9–13], or from the environment based on the reward interpret

✉ Dmitry A. Simakov
dmsimak@gmail.com

Ludmila B. Chernyakhovskaya
tms@samgtu.ru

[1] Samara State Technical University, Samara, Russia

[2] Jena, Thuringen, Germany

mechanisms [14–17]. The later also allows to make an insertion into a non-fixed hole [18]. All the approaches are based on the different Artificial Intelligent (AI) and advanced statistical techniques like, e.g., fuzzy classifiers, neural networks, support vector machines, Gaussian mixtures model, and hidden Markov models.

The analytical background of the majority of investigations is the classical quasi-static approach [3]. The approach is done under the small angle approximation, which excludes three-point contact, and guarantees the two-point contact. The analytical approach was developed further by [19] by adding deformations into the consideration. In addition, the two-point contact was considered in [20–24]. More specifically, the required geometrical and kinematic characteristics, and force interactions between a peg and a hole at the contact points were defined for this process in [20] depending on angle γ between the axes. Alternatives for relative orientation of parts during automatic assembly were considered in [21–24], and criteria for identifying them were specified.

The condition of two-point contact sets obvious limitations on the gap size and on the precision of the control of the initial angle between the parts, that is not systematically addressed. This is an important topic because for the very small gaps, there will be a three-point contact before the insertion starts, during which an alignment of the axis of peg at the edge of the hole is occurred. This phase is called peg-on-hole.

Peg with the three-point contact with the hole has three degrees of freedom, and its position is characterized with three generalized coordinates called Euler angles. They are: (i) nutation angle γ describing planar motion of aligning parts also called align, (ii) precession angle ψ describing rotational motion around hole axis also called slide, and (iii) self-rotation angle φ describing rotational motion of the peg about its axis also called slip. Align is purely a planar motion with reduction of angle γ, so both rotations are not directly involved in it. However, they have a dynamic effect on the process. This effect could become important for accidental slips and slides during align, and can also be used intentionally to decrease the jammings.

There are quite a few studies devoted to analysing motion of peg with three-point contact in Russian-speaking segment this work took inspiration from. The simplest is the approach with one degree of freedom. Directions of all interaction forces in this case were defined, and trajectories of all peg points and velocities of the contact were determined in [25, 26]; differential equations of peg motion characterizing alignment process were made [27]. The reasons of the parts' seizure were considered in detail, including action of gravity on the movable part producing considerable forces of interaction between a peg and a hole at the contact points. A potential reduction of this effect was analysed through changing a position of the movable part center of gravity [28, 29].

Works [30–33] present a mathematical model of aligning the parts by use of a device transmitting vibration to a hole. Calculations presented in these papers define a position of the peg mass center relative to a vibrating hole. However, this model is inadequate to determine a position of peg as a solid body.

An assembly process involving transmission of rotating motion to peg, a second degree of freedom, was studied in works [34–36]. Here the properties of gyroscope, a body that has the only stationary point, are attributed to a peg. It simplifies calculations for educative purposes, however, the description of forces is limited for academic or industrial applications.

[37, 38] made a first attempt among the English-speaking publication to consider the kinematics of three-point contacts and to determine the direction of the normal reaction forces. In their approach, the high stability of the assembly process starting with three-point contact was recognized, however, the normal reaction forces were not considered quantitatively, and the friction forces were not determined at all.

The model in [38] allowed to compare the contact reaction for the two situations of the alignments: with and without uniform sliding. The comparison showed that the slipping rotation during the alignment decreases reaction forces and therefore, the risk of jamming.

A more recent publication on the three-point contact was done by [7]. The modelling of the mechanics was meant to be a partial case of [38]. It included the interconnection between the alignment motion, reaction forces, the external forces for one degree of freedom, and the friction forces were suggested to get found experimentally. However, the directional cosines of the normal reaction forces and of the friction forces were not identified correctly.

Work [39] introduced the first analytical solution for the three point-contact alignment, which included rigorous solution based on analytical mechanics. The approach was developed for two of three degrees of freedom, namely align and slide. The reaction forces, including the normal reaction and friction forces, were derived based on the laws of geometry and analytical mechanics. As the next step, generalized coordinates and forces were identified for these two degrees of freedom. This allowed to derive a particular case of Lagrange system of differential equation for this particular case, a so-called Dynamic Differential Equations (DDE) of a system. This set of equations defines the full dynamic of the system, including interconnection between (i) the external influences, e.g., forces and torques of a manipulator; (ii) contact reactions: forces and torques at the contact points; as well as (iii) kinematic motion law of the parts. In other words, DDE allows to derive from the law of change of one of these sets the laws of change of the other two.

The freely moving body has six degrees of freedom: three planar and three rotational motions. Each contact point reduces one of the degrees of freedom, it means that the motion of peg-on-hole with three-point contact has three degrees of

freedom. This paper extends the study made in paper [38] by adding the third degree of freedom into DDE. It allows to consider the peg-on-hole motion in the most general case, when the forces, transfer all three types of peg-on-hole movements allowed by connections: align, slip, and slide.

The main part of the work is devoted to the step-by-step derivation of DDE in Section 3. This includes the study of directions of velocities, normal reactions, and friction forces at the contact points.

The goal pursued with DDE in this paper is addressing three major problems of the process for automated assembly of cylindrical parts:

1. Determining patterns of peg movement that facilitates alignment of the parts when all three generalized coordinates (Fig. 1) change: nutation angle $\gamma = \gamma(t)$, precession angle $\psi = \psi(t)$, and self-rotation angle $\varphi = \varphi(t)$.
2. Determining forces acting on peg at the points of contact and potentially preventing alignment of the parts.

Two example cases of solution of these problems were considered: (i) reaction forces for relative large alignment angle during uniform alignment and slip $\dot{\gamma} = \text{const}, \dot{\varphi} = \text{const}, \dot{\psi} = 0$ in comparison to the case without slip $\dot{\gamma} = \text{const}, \dot{\varphi} = 0, \dot{\psi} = 0$; (ii) the kinematics and directional cosines were studied for the small alignment angle approximation, and the reaction forces were analysed. The second example is also intended to give a simple insight into the principles behind DDE.

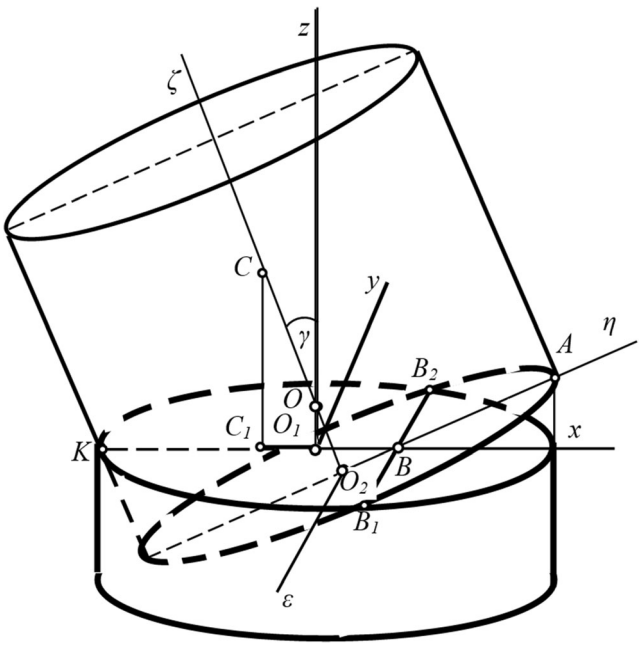

Fig. 1 Position of moving coordinate system $O_2\varepsilon\eta\zeta$ relative to fixed system O_1xyz at the beginning of alignment

2 Methodology and methods

Analysis of motion that enables alignment of a peg with a vertically fixed hole uses common patterns of mechanical movement of a solid body with the three degrees of freedom: nutation angle γ, precession angle ψ, and self-rotation angle φ.

All necessary characteristics of such motion might be obtained applying differential equations of the mass center movement (1) and Lagrange differential Eq. (2).

$$m\frac{d^2x_c}{dt^2} = \sum F_{kx}; \quad (1)$$
$$m\frac{d^2y_c}{dt^2} = \sum F_{ky};$$
$$m\frac{d^2z_c}{dt^2} = \sum F_{kz};$$

$$\frac{d}{dt}\frac{\partial T}{\partial \dot{\gamma}} - \frac{\partial T}{\partial \gamma} = Q_\gamma;$$
$$\frac{d}{dt}\frac{\partial T}{\partial \dot{\psi}} - \frac{\partial T}{\partial \psi} = Q_\psi; \quad (2)$$
$$\frac{d}{dt}\frac{\partial T}{\partial \dot{\phi}} - \frac{\partial T}{\partial \phi} = Q_\phi,$$

where F_{kx}, F_{ky}, and F_{kz} are the projections of the external forces k on the axes x, y, and z correspondingly. T is a kinematic energy of the peg during the motion, Q_γ, Q_ψ, and Q_φ are generalized forces of Lagrange.

Three coordinate systems are canonical to use for these three motions of the system: (i) fixed system of coordinates O_1xyz (see, e.g., Fig. 1), which are used in the definition of Lagrange equations; (ii) coordinate system O_1hez (see, e.g., Fig. 2) performing precession motion ψ with the peg around hole axis, in which peg could be considered without precession; and (iii) moving coordinate system $O_2\varepsilon\eta\zeta$ associated with peg, performing nutation motion γ. In this system, the self-rotational motion of peg around $O_2\zeta$ is considered. These coordinate systems are used to consider three generalized motions independently. Mathematically, transitions from (iii) to (ii), and from (ii) to (i) include nutation and precession motions into consideration consequently. The coordinate system O_1hez is the most convenient to describe the dynamics, since the most essential geometric and dynamical connections depend on the alignment angle γ. Thus, we use coordinates h and z to describe the dynamics and geometry in DDE (29).

Now, the left and right parts of (1) and (2) will be considered separately in order to derive DDE (29).

2.1 The left parts of mass center equations

The left parts of the first three differential equations (1) are the time derivatives from coordinates x_c, y_c, and z_c of the peg mass

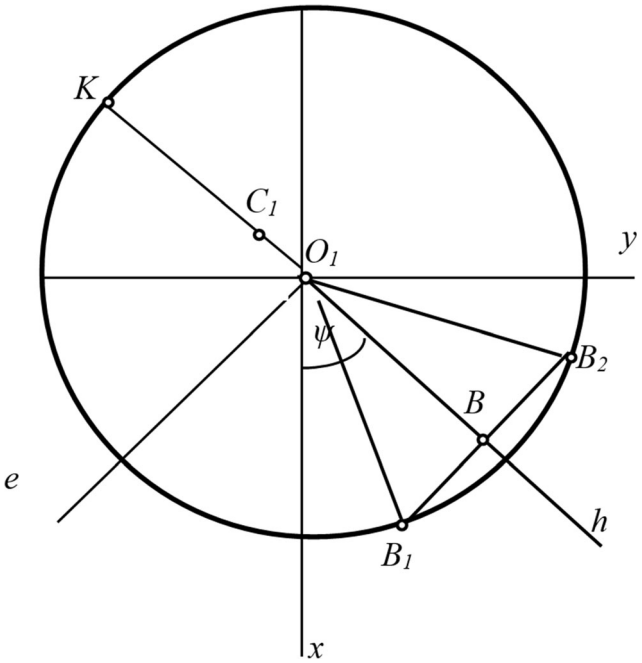

Fig. 2 Position of moving coordinate system O_1eh relative to fixed coordinate system O_1xy

center that are the functions of generalized coordinates γ, ψ, and φ.

The peg position in the process of aligning is defined relative to the fixed system of coordinates O_1xyz (see Fig. 1), the beginning of which coincides with center O_1 of the hole aperture edge, axis O_1z is directed along the hole axis, coordinate plane O_1xz passes through the hole axis, and the peg axis in the initial position of the parts, axis O_1x is the line of intersection of this plane with the horizontal plane of the edge, it coincides with the hole diameter, axis O_1y is perpendicular to plane O_1xz.

A moving coordinate system $O_2\varepsilon\eta\zeta$ (Fig. 1) is associated to the peg, with the beginning at the center of its aligned end, axis $O_2\zeta$ is directed along the peg axis, coordinate plane $O_2\zeta\eta$ passes through axes of the parts and is a principal plane of their symmetry in the course of alignment, axis $O_2\eta$ coincides with the diameter of a peg located in the plane of symmetry, axis $O_2\varepsilon$ is perpendicular to plane $O_2\zeta\eta$. When the peg moves, axis $O_2\varepsilon$ remains parallel to segment B_1B_2, axis $O_2\eta$ remains perpendicular to this segment.

To define a position of peg during its rotation about the sleeve axis, an auxiliary system of coordinates O_1ehz is used, with the beginning at point O_1. Axis O_1h is a line of intersection of the parts' plane of symmetry with the horizontal plane of the hole and forms angle ψ with fixed axis O_1x. Axis O_1e is perpendicular to plane O_1hz (see Fig. 2). Coordinates of mass center relative to fixed system of coordinates O_1xyz, defined in work [18], are as follows:

$$\begin{aligned} x_c &= -O_1C_1\cos\psi = -(0.5H-a_2)\sin\gamma\cos\psi = h_c\cos\psi;\\ y_c &= -O_1C_1\sin\psi = -(0.5H-a_2)\sin\gamma\sin\psi = h_c\sin\psi;\\ z_c &= (0.5H-a_2)\cos\gamma + a_1. \end{aligned} \tag{3}$$

where $a_1 = OO_1 = \frac{d-D\cos\gamma}{2\sin\gamma}$ is a distance between point O of intersection of the parts' axes and center O_1 of the hole edge circumference, and $a_2 = OO_2 = \frac{D-d\cos\gamma}{2\sin\gamma}$ —distance between point O and center O_2 of the aligned peg end.

In Eq. (3) and the corresponding expressions, the same notations are used as defined in the introduction: H is a height of the peg, D and d are diameters of hole and peg correspondingly.

The obtained values of the peg mass center coordinates (3) allow to transform the left parts of differential equations of the mass center movement (1)

$$\frac{d^2x_c}{dt^2} = \frac{dh_c}{d\gamma}\cos\psi\ddot{\gamma} - h_c\sin\psi\ddot{\psi} + \frac{d^2h_c}{d\gamma^2}\cos\psi\dot{\gamma}^2 - h_c\cos\psi\dot{\psi}^2 - 2\frac{dh_c}{d\gamma}\sin\psi\dot{\gamma}\dot{\psi}; \tag{4.1}$$

$$\frac{d^2y_c}{dt^2} = \frac{dh_c}{d\gamma}\sin\psi\ddot{\gamma} + h_c\cos\psi\ddot{\psi} + \frac{d^2h_c}{d\gamma^2}\sin\psi\dot{\gamma}^2 - h_c\sin\psi\dot{\psi}^2 + 2\frac{dh_c}{d\gamma}\cos\psi\dot{\gamma}\dot{\psi}; \tag{4.2}$$

$$m\frac{d^2z_c}{dt^2} = m\left(\frac{d^2z_c}{d\gamma^2}\dot{\gamma}^2 + \frac{dz_c}{d\gamma}\ddot{\gamma}\right). \tag{4.3}$$

2.2 Left parts of Lagrange equations

The left parts of Lagrange equations (2) used in DDE (29) shall be obtained through transforming kinetic peg energy,

$$T = \frac{mV_c^2}{2} + \frac{I_{c\varepsilon}\dot{\gamma}^2}{2} + \frac{I_z\dot{\psi}^2}{2} + \frac{I_\zeta\dot{\varphi}^2}{2}, \tag{5}$$

where m—mass of a peg, V_c – a velocity of its mass center, $\dot{\gamma}$ —angular velocity of planar motion, $\dot{\psi}$ —angular velocity of rotation motion of peg about hole axis, $\dot{\varphi}$ angular velocity of self-rotation, $I_{c\varepsilon}$—inertia moment of peg relative to axis $C\varepsilon$, passing through its mass center perpendicular to the parts' plane of symmetry. I_Z *is* inertia moment of peg relative to hole axis O_1z, I_ζ—inertia moment of peg relative to figure rotation axis $O_2\zeta$.

Here, $I_{c\varepsilon} = \frac{m}{12}\left(3R^2 + H^2\right)$ is a central moment of peg inertia relative to axis $C\varepsilon$, passing through the peg mass center perpendicular to its plane of symmetry, $I_\zeta = \frac{mR^2}{2}$ is a moment of peg inertia relative to its axis $O_2\zeta$, $I_z = I_{c\eta}\sin^2\gamma + I_\zeta\cos^2\gamma$

$+mh_c^2$ is a moment of peg inertia relative to hole axis O_1z, which is a variable value that depends on angle γ between axes.

Mass center velocity is expressed through its projections to fixed axes of coordinates O_1xyz

$$V_{cx} = \frac{dx_c}{dt} = \frac{dh_c}{d\gamma}\cos\psi\,\dot{\gamma} - h_c\sin\psi\,\dot{\psi};$$

$$V_{cy} = \frac{dy_c}{dt} = \frac{dh_c}{d\gamma}\sin\psi\dot{\gamma} + h_c\cos\psi\,\dot{\psi};$$

$$V_{cz} = \frac{dz_c}{d\gamma}\dot{\gamma};$$

where values h_c and z_c are defined by expressions (3). Hence,

$$V_c^2 = \left(\frac{dx_c}{dt}\right)^2 + \left(\frac{dy_c}{dt}\right)^2 + \left(\frac{dz_c}{dt}\right)^2 = \left[\left(\frac{dh_c}{d\gamma}\right)^2 + \left(\frac{dz_c}{d\gamma}\right)^2\right]\dot{\gamma}^2 + h_c^2\dot{\psi}^2.$$

Then, kinetic energy (5) shall be as follows

$$T = \frac{m}{2}\left\{\left[\left(\frac{dh_c}{d\gamma}\right)^2 + \left(\frac{dz_c}{d\gamma}\right)^2\right]\dot{\gamma}^2 + h_c^2\dot{\psi}^2\right\} + \frac{I_{c\varepsilon}\dot{\gamma}^2}{2} + \frac{I_z\dot{\psi}^2}{2} + \frac{I_\zeta\dot{\varphi}^2}{2}. \quad (6)$$

After kinetic energy is properly transformed, the left parts of Lagrange equations shall have the following values:

$$\frac{d}{dt}\frac{\partial T}{\partial\dot{\gamma}} - \frac{\partial T}{\partial\gamma} = m\left[\left(\frac{dh_c}{d\gamma}\right)^2 + \left(\frac{dz_c}{d\gamma}\right)^2\right]\ddot{\gamma} + I_{c\varepsilon}\ddot{\gamma} + m\left(\frac{dh_c}{d\gamma}\frac{d^2h_c}{d\gamma^2} + \frac{dz_c}{d\gamma}\frac{d^2z_c}{d\gamma^2}\right)\dot{\gamma}^2 - \left[m\frac{dh_c}{d\gamma}\frac{d^2h_c}{d\gamma^2} + 0.5\frac{dI_{cz}}{d\gamma}\right]\dot{\psi}^2; \quad (7.1)$$

$$\frac{d}{dt}\frac{\partial T}{\partial\dot{\psi}} - \frac{\partial T}{\partial\psi} = \left(mh_c^2 + I_z\right)\ddot{\psi} + \frac{dI_z}{d\gamma}\dot{\gamma}\dot{\psi}; \quad (7.2)$$

$$\frac{d}{dt}\frac{\partial T}{\partial\dot{\varphi}} - \frac{\partial T}{\partial\varphi} = I_\zeta\frac{d^2\varphi}{dt^2}. \quad (7.3)$$

2.3 Right parts of mass center equations

The right parts of differential equations of mass center motion (1.1), (1.2), and (1.3) constitute the sums of projections to fixed axes of coordinates of all forces that act upon peg, namely, assembling forces, peg gravity force, and normal reactions and friction forces applied at the contact points.

Assembling forces for aligning parts are known values that depend on a method of assembly and assembly device used. Normal reactions and friction forces characterizing interaction forces between the parts shall be defined.

Directions of normal reactions shall be defined by location of contact points, and the value of each contact point depends on common patterns of motion. Normal reaction $\overline{N}_K$ is directed perpendicular to the peg generating line; its projections to the fixed coordinate axes are equal to.

$$N_{Kx} = N_K\cos\gamma\cos\psi; \quad N_{Ky} = N_K\cos\gamma\sin\psi; \quad N_{Kz} = N_K\sin\gamma. \quad (8)$$

Lines of action of normal reactions $\overline{N}_{B1}$, $\overline{N}_{B2}$ at symmetric points of contact B_1 and B_2 pass through point O of peg and hole axes' intersection [18], and their direction cosines shall be defined from geometrical ratios. They should have the following values after transformations:

$$\cos\alpha_{B1}^N = -\left(\frac{S_1\cos\psi + b\sin\psi}{B_1}\right); \quad \cos\alpha_{B2}^N = -\left(\frac{S_1\cos\psi - b\sin\psi}{B_1}\right);$$
$$\cos\beta_{B1}^N = -\left(\frac{S_1\sin\psi - b\cos\psi}{B_1}\right); \quad \cos\beta_{B2}^N = -\left(\frac{S_1\sin\psi + b\cos\psi}{B_1}\right);$$
$$\cos\lambda_{B1}^N = \frac{a_1}{B_1}; \quad \cos\gamma_{B2}^N = \frac{a_1}{B_1}; \quad (9)$$

where (Fig. 3) $b = BB_1 = BB_2$; $B_1 = OB_1 = OB_2 = \sqrt{0.25D^2 + a_1^2}$.

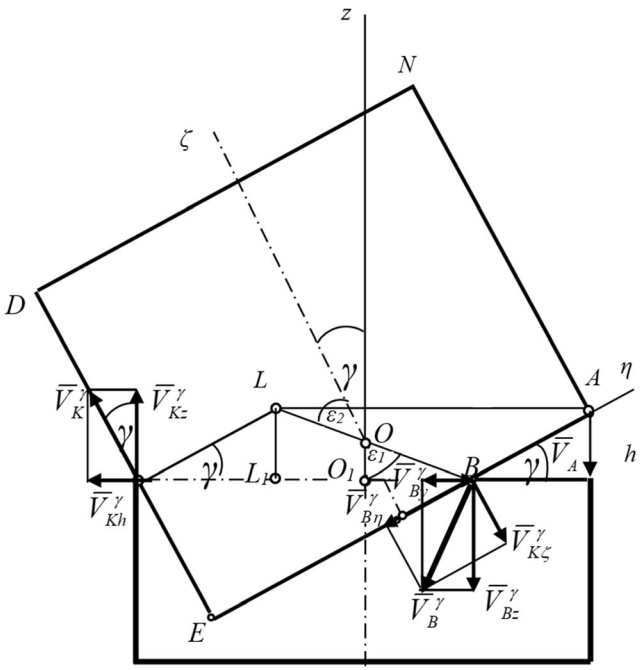

Fig. 3 Projections of the velocities of the planar motion onto axis systems O_1y, O_1z, and $O_2\eta$, $O_2\zeta$

Hence, projections of normal reactions shall be written as follows.

$$\begin{array}{lll} N^x_{B1} = N_{B1}\cos\alpha^N_{B1}; & N^x_{B2} = N_{B2}\cos\alpha^N_{B2}; & N^x_K = N_K\cos\alpha^N_K; \\ N^y_{B1} = N_{B1}\cos\beta^N_{B1}; & N^y_{B2} = N_{B2}\cos\beta^N_{B2}; & N^y_K = N_K\cos\beta^N_K; \\ N^z_{B1} = N_{B1}\cos\lambda^N_{B1}; & N^z_{B2} = N_{B2}\cos\lambda^N_{B2}; & N^z_K = N_K\cos\lambda^N_K. \end{array}$$

The direction of friction force is always opposite to the absolute velocity of the point of its application that involves determining the values of velocities of contact points of parts B_1, B_2, and K.

An absolute velocity of each point of peg shall be equal to vector sum of velocities of all component motions $\overline{V} = \overline{V}^{\gamma} + \overline{V}^{\psi} + \overline{V}^{\varphi}$; where $\overline{V}^{\gamma}$ is velocity of planar motion, $\overline{V}^{\psi}$ and $\overline{V}^{\varphi}$ are rotation velocities of points about hole and peg axes, respectively.

Planar motion. When only single angle γ is changing, the peg makes a planar motion which is characterized by the motion of its cross-section in the symmetry plane. The velocities of the points of the peg located in the plane symmetry are defined as rotational around the instantaneous center of velocities, located at the intersection of the perpendiculars to the velocities $\overline{V}_K$ and $\overline{V}_A$.

Velocities of symmetric points of contact B_1 and B_2 are equal to point B velocity, since they are located on one perpendicular line to the symmetry plane, passing through point B, hence, the values of the contact points' velocities shall be equal to

$$V^{\gamma}_{B1} = V^{\gamma}_{B2} = V^{\gamma}_B = BL\,\dot{\gamma}; \quad V^{\gamma}_K = KL\,\dot{\gamma}.$$

Projections of velocities $\overline{V}^{\gamma}_{B1}, \overline{V}^{\gamma}_{B2}, \overline{V}^{\gamma}_K$ of points B_1, B_2, and K on movable axes $O_2\eta$ and $O_2\zeta$ are equal to (see Fig. 3)

$$\begin{array}{l} V^{\gamma}_{B1\eta} = V^{\gamma}_{B2h} = -BL\,\dot{\gamma}\,cos\varepsilon_2 = -2a_2\,\dot{\gamma}; \\ V^{\gamma}_{B1\zeta} = V^{\gamma}_{B2\zeta} = -BL\,\dot{\gamma}\,sin\varepsilon_2 = -2S_2\,\dot{\gamma}. \\ V^{\gamma}_{K\zeta} = KL\,\dot{\gamma}; V^{\gamma}_{K\eta} = 0. \end{array} \tag{10}$$

Projections of these velocities $\overline{V}^{\gamma}_{B1}, \overline{V}^{\gamma}_{B2}, \overline{V}^{\gamma}_K$ to auxiliary axis O_1h are equal (see Fig.4) to

$$V^{\gamma}_{B1h} = V^{\gamma}_{B2h} = -BL\,\dot{\gamma}\cos\varepsilon_1 = -2a_1\,\dot{\gamma}; \tag{11}$$

$$V^{\gamma}_{Kh} = -KL\,\dot{\gamma}\sin\gamma.$$

These expressions include (see Fig.3) ε_1—angle between segment BL and axis of hole, ε_2—angle between segment BL and peg axis, $\cos\varepsilon_1 = \frac{a_1}{OB}$; $\sin\varepsilon_1 = \frac{S_1}{OB}$; $\sin\varepsilon_2 = \frac{S_2}{OB}$; $\cos\varepsilon_2 = \frac{a_2}{OB}$; $B = OB = \sqrt{a_1^2 + S_1^2} = \sqrt{a_2^2 + S_2^2}$; $BL = 2OB = 2B$.

Projections of velocities $\overline{V}^{\gamma}_{B1}$, $\overline{V}^{\gamma}_{B2}, \overline{V}^{\gamma}_K$ to fixed axes O_1x, O_1y, and O_1z (Fig. 4) are equal to

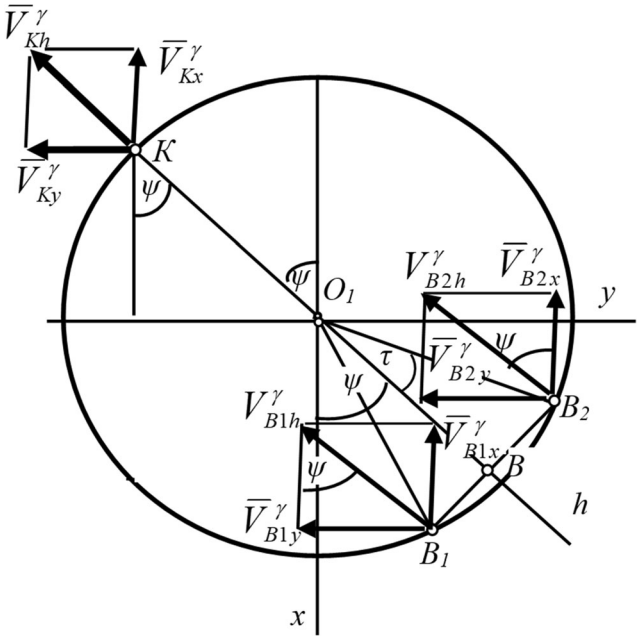

Fig. 4 Projections of velocities of planar potion on the fixed coordinate axes O_1x, O_1y

$$\begin{array}{ll} V^{\gamma}_{B1x} = V^{\gamma}_{B2x} = -V^{\gamma}_{B1h}\cos\psi = -2a_1\cos\psi\,\dot{\gamma}; & V^{\gamma}_{Kx} = -KL\sin\gamma\cos\psi\,\dot{\gamma}; \\ V^{\gamma}_{B1y} = V^{\gamma}_{B2y} = -V^{\gamma}_{B1h}\sin\psi = -2a_1\sin\psi\,\dot{\gamma}; & V^{\gamma}_{Ky} = -KL\sin\gamma\sin\psi\,\dot{\gamma}; \\ V^{\gamma}_{B1z} = V^{\gamma}_{B2z} = -2S_1\,\dot{\gamma}. & V^{\gamma}_{Kz} = KL\,\dot{\gamma}\cos\gamma. \end{array} \tag{12}$$

Rotation about hole axis occurs with angular velocity of $\dot{\psi} = \frac{d\psi}{dt}$. Velocities of contact points in this movement are located in the fixed plane O_1xy, directed (see Fig.5) at tangents to the hole aperture edge circumference and at all contact points are equal in magnitude

$$V^{\psi}_{B1} = V^{\psi}_{B2} = V^{\psi}_K = 0.5D\dot{\psi}.$$

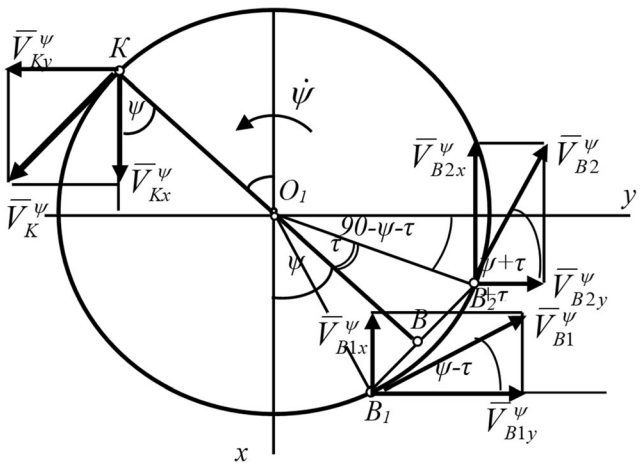

Fig. 5 Projections of velocities of the contact points during the rotation around hole's axis onto axes O_1x and O_1y

Projections of these velocities to the fixed axes of coordinates O_1x and O_1y (Fig. 5) taking values of $\sin\tau = \frac{b}{0.5D}$ and $\cos\tau = \frac{S_1}{0.5D}$ into account shall be transformed to the following form:

$$\begin{aligned} &V^{\psi}_{B1x} = -(S_1\sin\psi - b\cos\psi)\,\dot{\psi}; \quad V^{\psi}_{B2x} = -(S_1\sin\psi + b\cos\psi)\,\dot{\psi};\\ &V^{\psi}_{Kx} = 0.5D\sin\psi\,\dot{\psi}; V^{\psi}_{B1y} = (S_1\cos\psi + b\sin\psi)\,\dot{\psi};\\ &V^{\psi}_{B2y} = (S_1\cos\psi - b\sin\psi)\,\dot{\psi}; V^{\psi}_{Ky} = -0.5D\cos\psi\,\dot{\psi};\\ &V^{\psi}_{B1z} = 0; V^{\psi}_{B2z} = 0; V^{\psi}_{Kz} = 0. \end{aligned} \tag{13}$$

To define projections of velocities $\overline{V}^{\psi}_{B1}$ and $\overline{V}^{\psi}_{B2}$ onto moving axes of coordinates $O_2\varepsilon$ and $O_2\eta$, they are first divided into two components. One of these components is parallel to axis O_1e, and the second one is parallel to axis O_1h (Fig. 6).

$$\overline{V}^{\psi}_{B1} = \overline{V}^{\psi}_{B1e} + \overline{V}^{\psi}_{B1h}; \quad \overline{V}^{\psi}_{B2} = \overline{V}^{\psi}_{B2e} + \overline{V}^{\psi}_{B2h}.$$

The values of these components define the projections of velocities to auxiliary axes O_2e and O_2h (see Fig. 6).

$$\begin{aligned} V^{\psi}_{B1e} &= -V^{\psi}_{B1}\cos\tau = -0.5D\dot{\psi}\frac{O_1B}{0.5D} = -S_1\dot{\psi};\\ V^{\psi}_{B2e} &= -V^{\psi}_{B2}\cos\tau = -0.5D\dot{\psi}\frac{O_1B}{0.5D} = -S_1\dot{\psi};\\ V^{\psi}_{B1h} &= V^{\psi}_{B1}\sin\tau = 0.5D\dot{\psi}\frac{BB_1}{0.5D} = b\dot{\psi};\\ V^{\psi}_{B2h} &= -V^{\psi}_{B2}\sin\tau = -0.5D\dot{\psi}\frac{BB_2}{0.5D} = -b\dot{\psi}. \end{aligned} \tag{14}$$

Components $\overline{V}^{\psi}_{B1h}$ and $\overline{V}^{\psi}_{B2h}$, in its turn, shall be decomposed into two components, one of which is parallel to peg $O_{2\zeta}$ axis, the second is parallel to axis $O_2\eta$

$$\overline{V}^{\psi}_{B1h} = \overline{V}^{\psi}_{B1\zeta} + \overline{V}^{\psi}_{B1\eta}; \quad \overline{V}^{\psi}_{B2h} = \overline{V}^{\psi}_{B2\zeta} + \overline{V}^{\psi}_{B2\eta}.$$

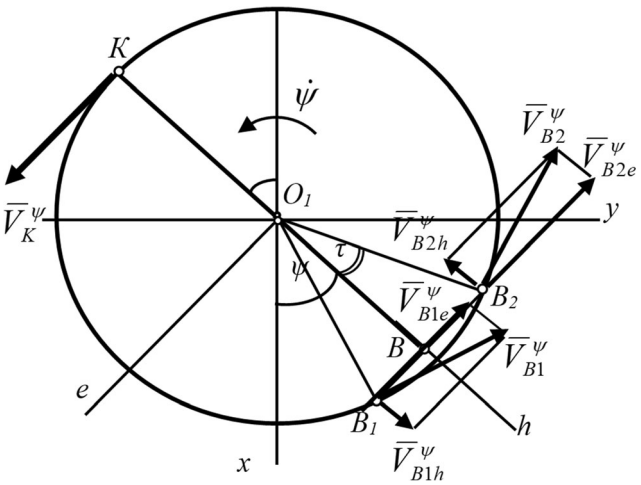

Fig. 6 Projections of the velocities of the contact points during the rotation around the hole's axis onto axes O_1e and O_1h

Thus, velocities $\overline{V}^{\psi}_{B1}$ and $\overline{V}^{\psi}_{B2}$ of points B_1 and B_2 of rotation peg motion around hole O_1z axis shall be decomposed into three components.

$$\overline{V}^{\psi}_{B1} = \overline{V}^{\psi}_{B1\varepsilon} + \overline{V}^{\psi}_{B1\zeta} + \overline{V}^{\psi}_{B1\eta}; \quad \overline{V}^{\psi}_{B2} = \overline{V}^{\psi}_{B2\varepsilon} + \overline{V}^{\psi}_{B2\zeta} + \overline{V}^{\psi}_{B2\eta}.$$

Projections of velocities $\overline{V}^{\psi}_{B1}$, $\overline{V}^{\psi}_{B2}$, and $\overline{V}^{\psi}_{K}$ to moving axes of coordinates $O_1\varepsilon$, $O_1\eta$, and $O_1\zeta$ shall be obtained through adding projections of their components (see Fig. 6).

$$\begin{aligned} &V^{\psi}_{B1\varepsilon} = V^{\psi}_{B1e} = -S_1\dot{\psi}; \quad V^{\psi}_{B2\varepsilon} = V^{\psi}_{B2e} = -S_1\dot{\psi}; \quad V^{\psi}_{K\varepsilon} = 0.5D\dot{\psi};\\ &V^{\psi}_{B1\eta} = V^{\psi}_{B1h}\cos\gamma = b\dot{\psi}\cos\gamma; \quad V^{\psi}_{B2\eta} = V^{\psi}_{B2h}\cos\gamma = -b\dot{\psi}\cos\gamma; \quad V^{\psi}_{K\eta} = 0;\\ &V^{\psi}_{B1\zeta} = -V^{\psi}_{B1h}\sin\gamma = -b\dot{\psi}\sin\gamma; \quad V^{\psi}_{B2\zeta} = V^{\psi}_{B2h}\sin\gamma = b\dot{\psi}\sin\gamma. \quad V^{\psi}_{K\zeta} = 0. \end{aligned} \tag{15}$$

Rotation of peg about its axis occurs with angular velocity $\dot{\varphi} = \frac{d\varphi}{dt}$.

Velocities $\overline{V}^{\varphi}_{K}$, $\overline{V}^{\varphi}_{B1}$, $\overline{V}^{\varphi}_{B2}$ of contact points K, B_1 and B_2 while moving are located in the plane of aligned peg end $O_2\varepsilon\eta$, and are equal in magnitude:

$$V^{\varphi}_{K} = V^{\varphi}_{B1} = V^{\varphi}_{B2} = 0.5d\dot{\varphi}.$$

Projections of these velocities to peg $O_2\zeta$ axis are equal to zero:

$$V^{\varphi}_{B1\zeta} = V^{\varphi}_{B2\zeta} = V^{\varphi}_{K\zeta} = 0.$$

Projections to moving axes $O_2\varepsilon$ and $O_2\eta$ (see Fig.7) are equal to.

$$\begin{aligned} &V^{\varphi}_{B1\varepsilon} = V^{\varphi}_{B1}\cos\beta = -0.5d\dot{\varphi}\frac{S_2}{0.5d} = -S_2\dot{\varphi}; \quad V^{\varphi}_{B1\eta} = V^{\varphi}_{B1}\sin\beta = 0.5d\dot{\varphi}\frac{b}{0.5d} = b\dot{\varphi}.\\ &V^{\varphi}_{B2\varepsilon} = -V^{\varphi}_{B1}\cos\beta = -0.5d\dot{\varphi}\frac{S_2}{0.5d} = -S_2\dot{\varphi}; \quad V^{\varphi}_{B2\eta} = V^{\varphi}_{B1}\sin\beta = -0.5d\dot{\varphi}\frac{b}{0.5d} = -b\dot{\varphi}.\\ &V^{\varphi}_{K\varepsilon} = 0.5d\dot{\varphi}; \quad V^{\varphi}_{K\eta} = 0. \end{aligned} \tag{16}$$

Each of $\overline{V}^{\varphi}_{B1\eta}$ and $\overline{V}^{\varphi}_{B2\eta}$ shall be divided into two components, one of which is directed along axis O_1h, the other is parallel to axis O_1z (see Fig. 8)

$$\overline{V}^{\varphi}_{B2\eta} = \overline{V}^{\varphi}_{B2h} + \overline{V}^{\varphi}_{B2z}.$$

Hence, velocity in each point may be presented as a sum of three components, two of which are located in horizontal plane O_1xy, and the third one is located vertically, i.e., parallel to axis O_1z.

$$\overline{V}^{\varphi}_{B1} = \overline{V}^{\varphi}_{B1e} + \overline{V}^{\varphi}_{B1h} + \overline{V}^{\varphi}_{B1z}; \quad \overline{V}^{\varphi}_{B2} = \overline{V}^{\varphi}_{B2e} + \overline{V}^{\varphi}_{B2h} + \overline{V}^{\varphi}_{B2z};$$

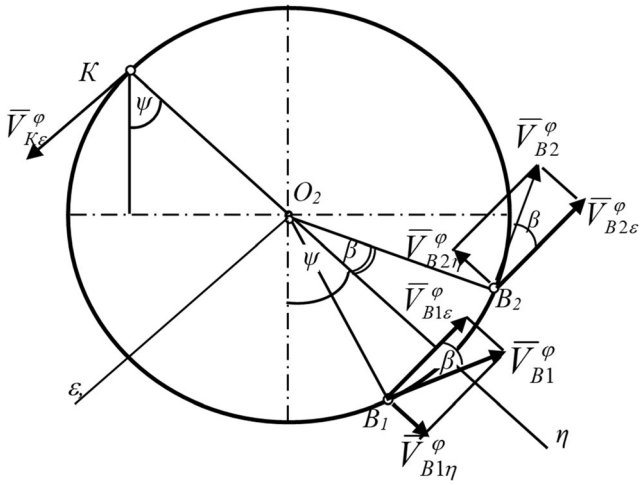

Fig. 7 Projections of self-rotation velocities to moving axes $O_2\varepsilon$ and $O_2\eta$

Projections of rotation velocities of the points to auxiliary axis O_1h are equal to.

$$V^{\varphi}_{B1h} = V^{\varphi}_{B1\eta}\cos\gamma = b\cos\gamma\dot{\varphi}; \quad V^{\varphi}_{B2h} = V^{\varphi}_{B2\eta}\cos\gamma = -b\cos\gamma\dot{\varphi}; \quad V^{\varphi}_{Kh} = 0; \tag{17}$$

Projections of velocities $\overline{V}^{\varphi}_{B1}$, $\overline{V}^{\varphi}_{B2}$, and $\overline{V}^{\varphi}_{K}$ to fixed axes of coordinates (Fig.8), after modifications shall be transformed to the form

$$\begin{gathered} V^{\varphi}_{B1x} = V^{\varphi}_{B1h}\cos\psi - V^{\varphi}_{B1e}\sin\psi = -(S_2\sin\psi - b\cos\gamma\cos\psi)\dot{\varphi}; \\ V^{\varphi}_{B1y} = V^{\varphi}_{B1h}\sin\psi + V^{\varphi}_{B1e}\cos\psi = (S_2\cos\psi + b\cos\gamma\sin\psi)\dot{\varphi}; \quad (18.1) \\ V^{\varphi}_{B1z} = V^{\varphi}_{B1\eta}\sin\gamma = b\sin\gamma\dot{\varphi}; \\ V^{\varphi}_{B2x} = -V^{\varphi}_{B2h}\cos\psi - V^{\varphi}_{B2e}\sin\psi = -(S_2\sin\psi + b\cos\gamma\cos\psi)\dot{\varphi}; \\ V^{\varphi}_{B2y} = -V^{\varphi}_{B2h}\sin\psi + V^{\varphi}_{B2e}\cos\psi = (S_2\cos\psi - b\cos\gamma\sin\psi)\dot{\varphi}; \quad (18.2) \\ V^{\varphi}_{B2z} = V^{\varphi}_{B2\eta}\sin\gamma = -b\sin\gamma\dot{\varphi}; \\ V^{\varphi}_{Kx} = 0.5d\sin\psi\dot{\varphi}; \; V^{\varphi}_{Ky} = -0.5d\cos\psi\dot{\varphi}; \; V^{\varphi}_{Kz} = 0. \quad (18.3) \end{gathered} \tag{18}$$

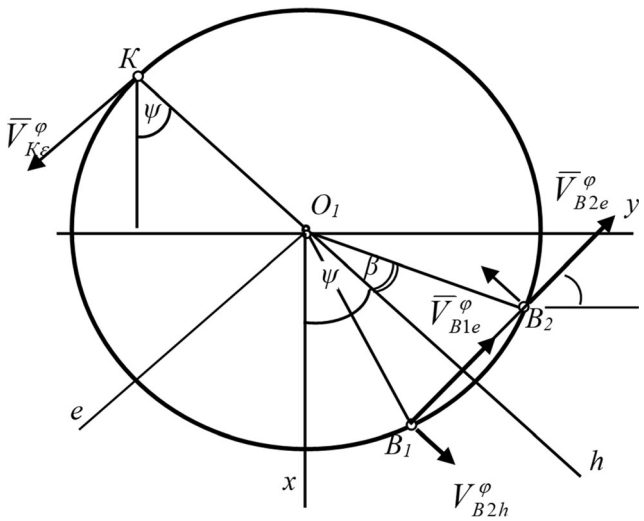

Fig. 8 Projections of self-rotation velocities to axes O_1e and O_1h

Projections of absolute velocities of each point of contact to fixed axes of coordinates O_1x, O_1y and O_1z shall be defined as sums of projections of velocity components based on Eqs. (12), (13), and (18), and shall be transformed to form:

$$\begin{gathered} V_{B1x} = V^{\gamma}_{B1x} + V^{\psi}_{B1x} + V^{\varphi}_{B1x} = -2a_1\cos\psi\dot{\gamma} - (S_1\sin\psi - b\cos\psi)\dot{\psi} - (S_2\sin\psi - b\cos\gamma\cos\psi)\dot{\varphi}; \\ V_{B1y} = V^{\gamma}_{B1y} + V^{\psi}_{B1y} + V^{\varphi}_{B1y} = -2a_1\sin\psi\dot{\gamma} + (S_1\cos\psi + b\sin\psi)\dot{\psi} + (S_2\cos\psi + b\cos\gamma\sin\psi)\dot{\varphi}; \quad (19.1) \\ V_{B1z} = V^{\gamma}_{B1z} + V^{\psi}_{B1z} + V^{\varphi}_{B1z} = -2S_1\dot{\gamma} + b\sin\gamma\dot{\varphi}; \\ V_{B2x} = V^{\gamma}_{B2x} + V^{\psi}_{B2x} + V^{\varphi}_{B2x} = -2a_1\cos\psi\dot{\gamma} - (S_1\sin\psi + b\cos\psi)\dot{\psi} - (S_2\sin\psi + b\cos\gamma\cos\psi)\dot{\varphi}; \\ V_{B2y} = V^{\gamma}_{B2y} + V^{\psi}_{B2y} + V^{\varphi}_{B2y} = -2a_1\sin\psi\dot{\gamma} + (S_1\cos\psi + b\sin\psi)\dot{\psi} + (S_2\cos\psi - b\cos\gamma\sin\psi)\dot{\varphi}; \quad (19.2) \\ V_{B2z} = V^{\gamma}_{B2z} + V^{\psi}_{B2z} + V^{\varphi}_{B2z} = -2S_1\dot{\gamma} - b\sin\gamma\dot{\varphi}; \\ V_{Kx} = V^{\gamma}_{Kx} + V^{\psi}_{Kx} + V^{\varphi}_{Kx} = -KL\sin\gamma\cos\psi\dot{\gamma} + 0.5D\sin\psi\dot{\psi} + 0.5d\sin\psi\dot{\varphi}; \\ V_{Ky} = V^{\gamma}_{Ky} + V^{\psi}_{Ky} + V^{\varphi}_{Ky} = -KL\sin\gamma\sin\psi\dot{\gamma} - 0.5D\cos\psi\dot{\psi} - 0.5d\cos\psi\dot{\varphi}; \quad (19.3) \\ V_{Kz} = V^{\gamma}_{Kz} + V^{\psi}_{Kz} + V^{\varphi}_{Kz} = KL\dot{\gamma}\cos\gamma. \end{gathered} \tag{19}$$

Projections of absolute velocities of contact points to moving axes of coordinates $O_2\varepsilon$ and $O_2\eta$ shall be determined based on Eqs. (11), (14), and (17).

$$\begin{gathered} V_{B1\varepsilon} = V^{\gamma}_{B1\varepsilon} + V^{\psi}_{B1\varepsilon} + V^{\varphi}_{B1\varepsilon} = -S_1\dot{\psi} - S_2\dot{\varphi}; \\ V_{B1\eta} = V^{\gamma}_{B1\eta} + V^{\psi}_{B1\eta} + V^{\varphi}_{B1\eta} = -2a_2\dot{\gamma} + b\cos\gamma\dot{\psi} + b\dot{\varphi}; \quad (20.1) \\ V_{B2\varepsilon} = V^{\gamma}_{B2\varepsilon} + V^{\psi}_{B2\varepsilon} + V^{\varphi}_{B2\varepsilon} = S_1\dot{\psi} - S_2\dot{\varphi}; \\ V_{B2\eta} = V^{\gamma}_{B2\eta} + V^{\psi}_{B2\eta} + V^{\varphi}_{B2\eta} = -2a_2\dot{\gamma} - b\cos\gamma\dot{\psi} - b\dot{\varphi}; \quad (20.2) \\ V_{K\varepsilon} = V^{\gamma}_{K\varepsilon} + V^{\psi}_{K\varepsilon} + V^{\varphi}_{K\varepsilon} = 0.5D\dot{\psi} + 0.5d\dot{\varphi}; \quad (20.3) \\ V_{K\eta} = V^{\gamma}_{K\eta} + V^{\psi}_{K\eta} + V^{\varphi}_{K\eta} = 0. \end{gathered} \tag{20}$$

Projections of absolute velocities of contact points to auxiliary axis O_1h shall be determined based on Eqs. (11), (14), and (17)

$$\begin{gathered} V_{B1h} = V^{\gamma}_{B1h} + V^{\psi}_{B1h} + V^{\varphi}_{B1h} = -2a_1\dot{\gamma} + b\dot{\psi} + b\cos\gamma\dot{\varphi}; \\ V_{B2h} = V^{\gamma}_{B2h} + V^{\psi}_{B2h} + V^{\varphi}_{B2h} = -2a_1\dot{\gamma} - b\dot{\psi} - b\cos\gamma\dot{\varphi}; \\ V_{Kh} = V^{\gamma}_{Kh} + V^{\psi}_{Kh} + V^{\varphi}_{Kh} = -KL\sin\gamma\dot{\gamma}. \end{gathered} \tag{21}$$

The obtained values of projections of points B_1, B_2, and K velocities to axes of coordinates allow to identify directions of friction forces relative to the specified axes of coordinates using direction cosines that will be opposite in sign to direction cosines of the respective absolute velocities.

Direction cosines of friction forces relative to fixed axes of coordinates shall be defined by the following expressions

$$\begin{gathered} \cos\alpha^{F}_{B1} = -\frac{V_{B1x}}{V_{B1}}; \quad \cos\alpha^{F}_{B2} = -\frac{V_{B2x}}{V_{B2}}; \quad \cos\alpha^{F}_{K} = -\frac{V_{Kx}}{V_{K}}; \quad (22.1) \\ \cos\beta^{F}_{B1} = -\frac{V_{B1y}}{V_{B1}}; \quad \cos\beta^{F}_{B2} = -\frac{V_{B2y}}{V_{B2}}; \quad \cos\beta^{F}_{K} = -\frac{V_{Ky}}{V_{K}}; \quad (22.2) \\ \cos\lambda^{F}_{B1} = -\frac{V_{B1z}}{V_{B1}}; \quad \cos\lambda^{F}_{B2} = -\frac{V_{B2z}}{V_{B2}}; \quad \cos\lambda^{F}_{K} = -\frac{V_{Kz}}{V_{K}}; \quad (22.3) \end{gathered} \tag{22}$$

where $V = \sqrt{V_x^2 + V_y^2 + V_z^2}$ —modulus of velocity at the corresponding point.

As a result of the conducted analysis, the following directions were established: directions of (i) the perpendicular

reactions and of (ii) all the friction forces, direction cosines of which are defined with the expressions (19), and (22), correspondingly. Therefore, the right parts of the differential equations of the mass centers (1) make the following expressions, in which F_x^{as}, F_y^{as}, and F_z^{as} are the projections of the assembly forces on the fixed coordinate axes.

$$\begin{aligned}
\sum F_{kx} &= F_x^{as} + N_K\left(\cos\alpha_K^N + f\cos\alpha_K^F\right) + N_{B1}\left(\cos\alpha_{B1}^N + f\cos\alpha_{B1}^F\right) + N_{B2}\left(\cos\alpha_{B2}^N + f\cos\alpha_{B2}^F\right); \quad (23.1)\\
\sum F_{ky} &= F_y^{as} + N_K\left(\cos\beta_K^N + f\cos\beta_K^F\right) + N_{B1}\left(\cos\beta_{B1}^N + f\cos\beta_{B1}^F\right) + N_{B2}\left(\cos\beta_{B2}^N + f\cos\beta_{B2}^F\right); \quad (23.2)\\
\sum F_{kz} &= -mg + F_z^{as} + +N_K\left(\cos\beta_K^N + f\cos\beta_K^F\right) + N_{B1}\left(\cos\beta_{B1}^N + f\cos\beta_{B1}^F\right) + N_{B2}\left(\cos\beta_{B2}^N + f\cos\beta_{B2}^F\right). \quad (23.3)
\end{aligned} \tag{23}$$

2.4 Right parts of Lagrange equations

The right parts of Lagrange equations are the sums of moments of all forces applied to peg relative to pertinent rotation axes.

Generalized force Q_γ, the right part of the first Lagrange equation, is equal to the sum of moments of forces acting upon peg relative to instantaneous axis of rotation Ll, which passes through instantaneous center of velocities L perpendicular to the plane of parts symmetry O_1hz. Normal reactions intersect instantaneous axis of rotation; their moments relative to this axis are equal to zero. Thus, generalized force Q_γ is composed of moments of assembling forces, gravity force, and friction forces applied at the contact points.

$$Q_\gamma = m_{Ll}\left(\overline{F}^{as}\right) + m_{Ll}\left(m\overline{g}\right) + m_{Ll}\left(\overline{F}_K\right) + m_{Ll}\left(\overline{F}_{B1}\right) + m_{Ll}\left(\overline{F}_{B2}\right).$$

The moment of assembling force is a known value that depends on a method of assembly.

To determine gravity force $m\overline{g}$ moment and moments of friction forces $\overline{F}_K$, $\overline{F}_{B1}$, and $\overline{F}_{B2}$ relative to instantaneous axis Ll, axes of coordinates O_1h_1 and Lz_1, perpendicular to instantaneous axis of rotation, shall be associated with point L: axis Lh_1, parallel to axis O_1h, and axis Lz_1, parallel to hole axis O_1z (see Fig. 9).

Gravity force moment (see Fig. 9) relative to instantaneous axis is equal to

$$\begin{aligned}
&m_{Ll}\left(m\overline{g}\right) = -mgH_c = -mg(O_1L_1 - C_1O_1) =\\
&-mg(S_1 - h_c) = -mg[S_1 - (0.5H - a_2)\sin\gamma].
\end{aligned} \tag{24}$$

Moment of each friction force relative to instantaneous axis shall be defined by formula

$$m_{Ll}\left(\overline{F}\right) = h_1F_{z1} - z_1F_{h1}, \tag{25}$$

where h_1 and z_1 are coordinates of points for applying these forces in the specified system of coordinates (Fig.8), F_{z1} and F_{h1} are projections of friction forces to these axes.

Coordinates of contact points B_1, B_2, and K are equal to

$$\begin{aligned}
&h_{1B1} = h_{1B2} = h_{1B} = LB_3 = 2S_1; \quad h_{1K} = -KL_1 = -KL\cos\gamma;\\
&z_{1B1} = z_{1B2} = -L_1L = -2a_1; \qquad z_{1K} = -KL\sin\gamma;
\end{aligned} \tag{26}$$

Axis of coordinates Lz_1 is parallel to axis O_1z, hence, direction cosines of friction forces relative to axis Lz_1 are equal to direction cosines of angles relative to axis O_1z, the values of which are as follows (19)

$$\cos\lambda_{B1}^F = -\frac{V_{B1z}}{V_{B1}}; \quad \cos\lambda_{B2}^F = -\frac{V_{B2z}}{V_{B2}}; \quad \cos\lambda_K^F = -\frac{V_{Kz}}{V_K}.$$

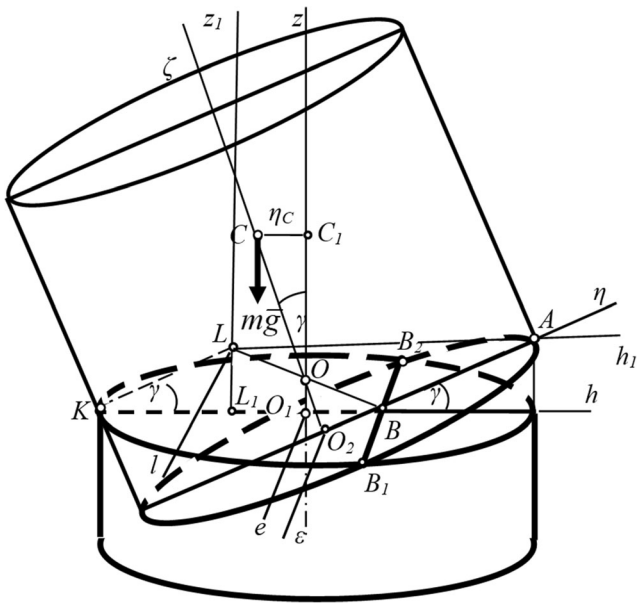

Fig. 9 Coordinates of the contact points in the coordinate system Llh_1z_1 associated to the instantaneous center of velocities of the planar motion

After substituting all components into formula (25) and further transformations, moments of friction forces $\overline{F}_K$, $\overline{F}_{B1}$, and $\overline{F}_{B2}$ relative to instantaneous axis of rotation shall be equal to

$$m_{Ll}\left(\overline{F}_K\right) = h_K F_{Kz} - z_K F_{Kh} = fN_K \frac{KL^2\dot{\gamma}}{V_K};$$
$$m_{Ll}\left(\overline{F}_{B1}\right) = h_{B1} F_{B1z} - z_{B1} F_{B1h} = fN_{B1} \frac{BL^2\dot{\gamma} - 2a_1 b\dot{\psi} - 2a_2 b\dot{\varphi}}{V_{B1}};$$
$$m_{Ll}\left(\overline{F}_{B2}\right) = h_{B2} F_{B2z} - z_{B2} F_{B2h} = fN_{B2} \frac{BL^2\dot{\gamma} + 2a_1 b\dot{\psi} + 2a_2 b\dot{\varphi}}{V_{B2}}.$$

Thus, generalized force of the first Lagrange equation is equal to

$$Q_\gamma = m_{Ll}\left(\overline{F}^{\text{as}}\right) - mg[S_1 - (0.5H - a_2)sin\gamma] + fN_K \frac{KL^2\dot{\gamma}}{V_K} + fN_{B1} \frac{BL^2\dot{\gamma} + 2a_1 b\dot{\psi} - 2a_2 b\dot{\varphi}}{V_{B1}} + fN_{B2}\left(\frac{BL^2\dot{\gamma} + 2a_2 b\dot{\varphi} + 2a_1 b\dot{\psi}}{V_{B2}}\right). \quad (27.1)$$

Generalized force Q_ψ in the second Lagrange equation is equal to the sum of moments of all these forces relative to the hole axis. Gravity force is parallel to the hole axis, normal reactions intersect it, thus, their moments are equal to zero. Moment of assembling forces $m_z\left(\overline{F}^{\text{as}}\right)$ depends on a method used for assembling.

Moment of each friction force shall be defined by formula

$$m_z\left(\overline{F}\right) = xF_y - yF_x;$$

where x and y are coordinates of contact points K, B_1, and B_2 in fixed system coordinates O_1xyz, values of which after transformations are equal to

$$x_{B1} = S_1\cos\psi + b\sin\psi; \quad x_{B2} = S_1\cos\psi - b\sin\psi; \quad x_K = -0.5D\cos\psi;$$
$$y_{B1} = S_1\sin\psi - b\cos\psi; \quad y_{B2} = S_1\sin\psi + b\cos\psi; \quad y_K = -0.5D\sin\psi.$$

Projections of friction forces to fixed axes of coordinates shall be expressed through normal reactions at contact points

$$F_{B1x} = fN_{B1}\cos\alpha^F_{B1}; \quad F_{B2x} = fN_{B2}\cos\alpha^F_{B2}; \quad F_{Kx} = fN_K\cos\alpha^F_K;$$
$$F_{B1y} = fN_{By}\cos\beta^F_{B1}; \quad F_{B2x} = fN_{B2}\cos\beta^F_{B2}; \quad F_{Ky} = fN_K\cos\beta^F_K;$$

where all direction cosines are defined by values (22).

After substituting all values and further transformations, moments of friction forces $\overline{F}_{B1}$, $\overline{F}_{B2}$, and $\overline{F}_K$ relative to axis O_1z shall have the following values.

$$m_z\left(\overline{F}_{B1}\right) = x_{B1}F_{B1y} - y_{B1}F_{B1x} = fN_{B1} \times \frac{2a_1 b\dot{\gamma} - \left(S_1S_2 + b^2\cos\gamma\right)\dot{\varphi} - 0.25D^2\dot{\psi}}{V_{B1}};$$
$$m_z\left(\overline{F}_{B2}\right) = x_{B2}F_{B2y} - y_{B2}F_{B2x} = -fN_{B2} \times \frac{2a_1 b\dot{\gamma} + \left(S_1S_2 + b^2\cos\gamma\right)\dot{\varphi} + 0.25D^2\dot{\psi}}{V_{B2}};$$
$$m_z\left(\overline{F}_K\right) = x_K F_{Ky} - y_K F_{Kx} = -fN_K \frac{0.25D^2\dot{\psi} + 0.25dD\dot{\varphi}}{V_K}.$$

Hence, generalized force of the second Lagrange equation shall be brought to the following form.

$$Q_\psi = m_z\left(\overline{F}^{\text{as}}\right) + m_z\left(\overline{F}_K\right) + m_L\left(\overline{F}_{B1}\right) + m_z\left(\overline{F}_{B2}\right) = m_z\left(\overline{F}^{\text{as}}\right) + fN_{B1}\frac{2a_1 b\dot{\gamma} - \left(S_1S_2 + b^2\cos\gamma\right)\dot{\varphi} - 0.25D^2\dot{\psi}}{V_{B1}} - fN_{B2}\frac{2a_1 b\dot{\gamma} + \left(S_1S_2 + b^2\cos\gamma\right)\dot{\varphi} + 0.25D^2\dot{\psi}}{V_{B2}} - fN_K\frac{0.25D^2\dot{\psi} + 0.25dD\dot{\varphi}}{V_K}. \quad (27.2)$$

Generalized force Q_φ of the third Lagrange equation is equal to the sum of moments of all forces applied to peg relative to peg axis $O_2\zeta$. Moments of gravity force and normal reactions are equal to zero, since lines of their action intersect this axis. Moments of friction forces relative to peg axis $O_2\zeta$ shall be defined by formula $m_\zeta(F) = \varepsilon F_\eta - \eta F_\varepsilon$.

Coordinates of contact points in moving system of coordinates $O_2\varepsilon\eta\zeta$ are equal to

$$\varepsilon_{B1} = BB_1 = b; \quad \varepsilon_{B2} = BB_2 = -b; \quad \varepsilon_K = 0;$$
$$\eta_{B1} = O_2B = S_2; \quad \varepsilon_{B2} = BB_2 = -b; \quad \eta_K = -0.5d.$$

Projections of friction forces are equal to

$$F_{B1\varepsilon} = fN_{B1}\cos\varepsilon^F_{B1}; \quad F_{B2\varepsilon} = fN_{B2}\cos\varepsilon^F_{B2}; \quad F_{K\varepsilon} = fN_K\cos\varepsilon^F_K;$$
$$F_{B1\eta} = fN_{By}\cos\eta^F_{B1}; \quad F_{B2\eta} = fN_{B2}\cos\eta^F_{B2}; \quad F_{K\eta} = fN_K\cos\eta^F_K;$$

where direction cosines of friction forces with axes $O_2\varepsilon$ and $O_2\eta$ are equal to

$$\cos\varepsilon_{B1}^{F}=\frac{S_1\dot{\psi}+S_2\dot{\varphi}}{V_{B1}};\quad \cos\eta_{B1}^{F}=\frac{2a_2\dot{\gamma}-b\cos\gamma\dot{\psi}-b\dot{\varphi}}{V_{B1}};$$

$$\cos\varepsilon_{K}^{F}=-\frac{0.5D\dot{\psi}+0.5d\dot{\varphi}}{V_K};\qquad \cos\varepsilon_{B2}^{F}=\frac{S_1\dot{\psi}+S_2\dot{\varphi}}{V_{B2}};$$

$$\cos\eta_{B2}^{F}=\frac{2a_2\dot{\gamma}+b\cos\gamma\dot{\psi}+b\dot{\varphi}}{V_{B2}};\cos\eta_{K}^{F}=0;$$

After transformations, moments of friction forces relative to peg axis $O_2\zeta$ shall be brought to the following form

$$m_\zeta(F_K)=-fN_K\frac{0.25d^2\dot{\varphi}+0.25dD\dot{\psi}}{V_K};$$
$$m_\zeta\left(\overline{F}_{B1}\right)=fN_{B1}\frac{2a_1b\dot{\gamma}-0.25d^2\dot{\varphi}-\left(S_1S_2+b^2\cos\gamma\right)\dot{\psi}}{V_{B1}};$$
$$m_\zeta\left(\overline{F}_{B2}\right)f=N_{B2}\frac{2a_1b\dot{\gamma}-0.25d^2\dot{\varphi}-\left(S_1S_2+b^2\cos\gamma\right)\dot{\psi}}{V_{B2}}.$$

Generalized force of the third Lagrange equation shall be as follows

$$Q_\varphi=m_\zeta\left(\overline{F}^{\text{as}}\right)+fN_{B1}\frac{2a_1b\dot{\gamma}-0.25d^2\dot{\varphi}-\left(S_1S_2+b^2\cos\gamma\right)\dot{\psi}}{V_{B1}}$$
$$+fN_{B2}\frac{2a_1b\dot{\gamma}-0.25d^2\dot{\varphi}-\left(S_1S_2+b^2\cos\gamma\right)\dot{\psi}}{V_{B2}}-fN_K\frac{0.25d^2\dot{\varphi}+0.25dD\dot{\psi}}{V_K};\tag{27.3}$$

where $m_\zeta\left(\overline{F}^{\text{as}}\right)$ is a moment of assembling force relative to peg axis $O_2\zeta$.

2.5 Dynamic differential equations (DDE)

Comprehensive analysis of peg motion enabled to define right (5) and left (28) parts of differential equations of mass center movement (1), and right (8) and left (28) parts of Lagrange equations (2). After equating corresponding values of these components, six differential equations shall be obtained (28).

$$m\left[\left(\frac{dh_c}{d\gamma}\right)^2+\left(\frac{dz_c}{d\gamma}\right)^2\right]\ddot{\gamma}+I_{cz}\ddot{\gamma}+m\left(\frac{dh_c}{d\gamma}\frac{d^2h_c}{d\gamma^2}+\frac{dz_c}{d\gamma}\frac{d^2z_c}{d\gamma^2}\right)\dot{\gamma}^2-\left[m\frac{dh_c}{d\gamma}\frac{d^2h_c}{d\gamma^2}+0.5\frac{dI_{cz}}{d\gamma}\right]\dot{\psi}^2=m_{Ll}\left(\overline{F}^{\text{as}}\right)-mg[S_1-(0.5H-a_2)\sin\gamma]$$
$$+fN_K\frac{KL^2\dot{\gamma}}{V_K}+fN_{B1}\frac{BL^2\dot{\gamma}+2a_1b\dot{\psi}-2a_2b\dot{\varphi}}{V_{B1}}+fN_{B2}\frac{BL^2\dot{\gamma}+2a_2b\dot{\varphi}+2a_1b\dot{\psi}}{V_{B2}}.\tag{28.1}$$

$$\left(mh_c^2+I_z\right)\ddot{\psi}+\frac{dI_z}{d\gamma}\dot{\gamma}\dot{\psi}\quad=m_z\left(\overline{F}^{\text{as}}\right)-fN_K\frac{0.25D^2\ddot{\psi}+0.25dD\ddot{\varphi}}{V_K}$$
$$+fN_{B1}\frac{2a_1b\dot{\gamma}-\left(S_1S_2+b^2\cos\gamma\right)\dot{\varphi}-0.25D^2\dot{\psi}}{V_{B1}}$$
$$-fN_{B2}\frac{2a_1b\dot{\gamma}+\left(S_1S_2+b^2\cos\gamma\right)\dot{\varphi}-0.25D^2\dot{\psi}}{V_{B2}};\tag{28.2}$$

$$I_\zeta\ddot{\varphi}\quad=\quad m_\zeta\left(\overline{F}^{\text{as}}\right)-fN_K\frac{0.25d^2\ddot{\varphi}+0.25dD\ddot{\psi}}{V_K}$$
$$+fN_{B1}\frac{2a_2b\dot{\gamma}+0.25d^2\dot{\varphi}-\left(S_1S_2+b^2\cos\gamma\right)\dot{\psi}}{V_{B1}}$$
$$-fN_{B2}\frac{2a_1b\dot{\gamma}-0.25d^2\dot{\varphi}-\left(S_1S_2+b^2\cos\gamma\right)\dot{\psi}}{V_{B2}}.\tag{28.3}$$

$$m[\frac{dh_c}{d\gamma}\cos\psi\ddot{\gamma}-h_c\sin\psi\ddot{\psi}+\frac{d^2h_c}{d\gamma^2}\cos\psi\dot{\gamma}^2-h_c\cos\psi\dot{\psi}^2-2\frac{dh_c}{d\gamma}\sin\psi\dot{\gamma}\dot{\psi}]=\tag{28.4}$$
$$=\quad F_x^{\text{as}}+N_K\left(\cos\alpha_K^N+f\cos\alpha_K^F\right)+N_{B1}\left(\cos\alpha_{B1}^N+f\cos\alpha_{B1}^F\right)$$
$$+N_{B2}\left(\cos\alpha_{B2}^N+f\cos\alpha_{B2}^F\right);$$

$$m[\frac{dh_c}{d\gamma}\sin\psi\ddot{\gamma}+h_c\cos\psi\ddot{\psi}+\frac{d^2h_c}{d\gamma^2}\sin\psi\dot{\gamma}^2-h_c\sin\psi\dot{\psi}^2+2\frac{dh_c}{d\gamma}\cos\psi\dot{\gamma}\dot{\psi}]=\tag{28.5}$$
$$F_y^{\text{as}}+N_K\left(\cos\beta_K^N+f\cos\beta_K^F\right)+N_{B1}\left(\cos\beta_{B1}^N+f\cos\beta_{B1}^F\right)$$
$$+N_{B2}\left(\cos\beta_{B2}^N+f\cos\beta_{B2}^F\right);$$

$$m(\frac{d^2z_c}{d\gamma^2}\dot{\gamma}^2+\frac{dz_c}{d\gamma}\ddot{\gamma})\quad=\quad-mg+F_z^{\text{as}}+N_K\left(cos\lambda_K^N+fcos\lambda_K^F\right)\tag{28.6}$$
$$+N_{B1}\left(cos\lambda_{B1}^N+fcos\lambda_{B1}^F\right)+N_{B2}\left(cos\lambda_{B2}^N+fcos\lambda_{B2}^F\right)$$

This is a system of Dynamic Differential Eqs. (28), and it is a mathematical model of process for aligning cylindrical parts in the most general way, when a peg, supported at the three points of the hole edge of vertically fixed hole, makes a compound motion characterized by three degrees of freedom. Such model may serve as a basis for considering all possible alternatives of vertical assembly schemes. A comparison of them will facilitate assessment of effect that rotatory motions have on reliability and quality of assembly.

2.6 Examples of application of DDE

DDE (28) is the general way to describe the mechanics of the peg-on-hole during three-point contact. One could distinguish different types of motion by implementing alignment of small angle approximation $\gamma = \gamma_0 + \varepsilon$. The expression for a_1 from (3) becomes:

$$a_1 = \frac{D\gamma_0\varepsilon}{2(\gamma_0 + \varepsilon)} \tag{29}$$

From here four stages of alignment could be identified: (i) small alignment angles $\varepsilon \ll \gamma_0 \ll 1$ with $a_1 \approx D\varepsilon/2 \approx 0$; (ii) medium alignment angles $\varepsilon \sim \gamma_0 \ll 1$ with $a_1 = \frac{D\gamma_0\varepsilon}{2(\gamma_0+\varepsilon)}$; (iii) larger alignment angles $\gamma_0 \ll \varepsilon \ll 1$ with $a_1 \approx D\gamma_0/2$ and (iv) large alignment angles $\varepsilon \sim 1$ with exact expression $a_1 = \frac{d-D\cos\varepsilon}{2\sin\varepsilon}$.

Based on this classification, two examples of DDE applications are considered. The first is the comparison of the reaction forces for the cases with and without rotational slip motion. The second is a small angle case for three degrees of freedom.

2.6.1 Analysis of the influence of the alignment with help of rotational motion

Based on the DDE (28), two cases of the assembly process were considered, and the dynamic reactions at the contact points under the assembly moment M_γ^{as} were established:

(i) with one degree of freedom, where differential equations of motion are obtained by substituting values $\varphi = 0$, $\dot{\varphi} = 0$, $\psi = 0$, and $\dot{\psi} = 0$ into system of DDE (28). Here the constant alignment angular velocity $\dot{\gamma} = -0,16\ s^{-1}$ is used;

(ii) with two degrees of freedom, where differential equations of motion are obtained by substituting values $\psi = 0$, $\dot{\psi} = 0$ into system of DDE (28). Here the constant alignment $\dot{\gamma} = -0,16\ s^{-1}$ and rotational $\dot{\varphi} = 2\ s^{-1}$ angular velocities are used.

The following set of parameters was considered for both cases: $D = 50$ mm, $d = 49.9$ mm, $H = 70$ mm, friction coefficient $f = 0.2$.

The system of equations, obtained by the mentioned substitutions allow to find an equation of peg alignment motion $\gamma = \gamma(t)$, and find the values of dynamic reactions, which correspond to this process. The differential equations were solved numerically based on standard Mathcad package.

The results are presented as a dependence between angle γ and value $n_K = \frac{R_K}{mg}$, which is an overall reaction at point K to peg normalized to the gravity force. Overall reaction $\overline{R}$ consists normal reaction $\overline{N}$ and friction force $\overline{F}$, and is their vector sum. Thus, $R_K = \sqrt{N_K^2 + F_K^2} = N_K\sqrt{1+f^2}$. As follows from the plot, the system reaches the maximal reaction forces when the alignment angle approaches the critical value $\gamma_0 = \arccos(d/D)$. Here peg-on-hole alignment phase finishes, because symmetric points of contact B_1 and B_2 becomes one at the opposite of contact point K, and the peg-in-hole insertion begins.

The results of the solution of the DDE are shown graphically for cases (i) and (ii), see Fig. 10. From the results it follows, that the reaction for the gamma values of ~0.15 during the alingmnent without peg rotation (i) is ~45, and is larger in comparison to the case with the peg rotation ~35.

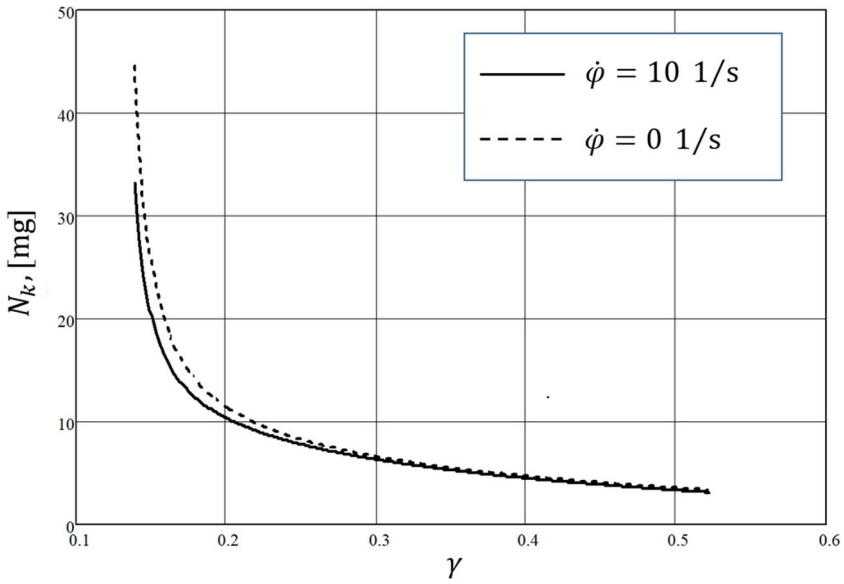

Fig. 10 Comparison of reaction force in point K during alignment between cases with and without rotational slip motion. $\dot{\gamma} = -0.16$

So the use of DDE could lead us to the conclusion that the peg rotation could reduce the contact forces during the alignment by factor of ~ 1.3.

To determine an impact of rotary motion of peg around its axis on the process of aligning parts, differential equations of peg motion with the two degrees of freedom: angle γ, characterizing planar motion, and self-rotation angle φ, specifying common patterns of the peg rotary motion around its axis, need to be written. Here, differential equations shall be obtained by substituting values $\psi = 0$, $\dot{\psi} = 0$ into equation (33). After all transformations five Eqs. (36) were compiled that define common patterns of motion of the peg with the two degrees of motion, which enable to write equations of peg motion and normal reactions at contact points depending on assembly forces applied.

2.6.2 Small alignment angles with three degrees of freedom

One of the most interesting cases for the peg-in-hole assembly is a state recognition. So it would be especially interesting to understand, what happens during transition from three-point contact to two-point contact. The mathematical condition for this is $\varepsilon \ll \gamma_0 \approx \frac{\Delta D}{D} \ll 1$, where $\Delta D = D - d$.

As an example, the following values for the parameters are considered (similarly to Section 2.6.2): $D = 50$ mm, $d = 49.9$ mm, $H = 70$ mm, friction coefficient $f = 0.2$, alignment rotational speed $\dot{\gamma} = -0.16\ \mathrm{s}^{-1}$.

Under these assumptions, the basic values get the following expressions:

$$a_1 \approx 0;\quad a_2 \approx 0; S_1 \approx D/2;\quad S_2 \approx D/2;\quad b \approx 0;\quad B_1 \approx D/2;\quad h_c \approx 0;$$
$$\frac{dh_c}{d\gamma} \approx -H/2;\quad \frac{d^2h_c}{d\gamma^2} \approx -D/2;\quad \frac{dz_c}{d\gamma} \approx D/2;\quad \frac{d^2z_c}{d\gamma^2} \approx D/\gamma_c. \tag{30}$$

These expressions show in particular, that for small angles the axes of the details are crossed at the center of peg base, and that two symmetrical points of contact B_1 and B_2 are reduced to a single point B, which is positioned at the opposite side of the base circle from the point K. Now the expressions (30) could be substituted into Eqs. (8–9) to find the approximate directional cosines for the normal reaction forces at the points of the contact:

$$\cos\alpha_{B_1}^N \approx \cos\alpha_{B2}^N \approx -\cos\psi;\quad \cos\beta_{B1}^N \approx \cos\beta_{B2}^N \approx -\sin\psi;\quad \cos\lambda_{B1}^N \approx \cos\lambda_{B2}^N \approx 0;$$
$$cos\alpha_K^N \approx cos\psi;\quad cos\beta_{B1}^N \approx sin\psi;\quad cos\lambda_K^N \approx \gamma_0. \tag{31}$$

Set of expression (31) could again be interpreted as the interaction of two horizontal bases of the peg and the hole. All the normal reaction forces are directed inside the plane of the hole base towards the hole center. The only exclusion is the small vertical component of the normal reaction at the point K. The reason of this vertical component is small misalignment γ_0 caused by the gap between the peg and the hole.

The expression of velocities components for the align motion, related to the nutation angle γ could be obtained by the substitution of (30) into (12):

$$V_{KZ}^{\gamma} \approx V_{KX}^{\gamma} \approx V_{KY}^{\gamma} \approx V_{B1X}^{\gamma} \approx V_{B1Y}^{\gamma} \approx V_{B2X}^{\gamma} \approx V_{B2Y}^{\gamma} \approx 0;\quad V_{B2Z}^{\gamma} \approx V_{B2Z}^{\gamma} \approx -D\dot{\gamma}. \tag{32}$$

The expressions (32) could be interpreted as a planar motion in a vertical plane around the point L which is reduced to the point K in this case. The reduced contact point B is the opposite side of the peg base circle with respect to point K, so the radius of the instantaneous rotation in this case is the peg diameter D.

The expression of velocities components for the slide motion, related to the precession angle ψ could be obtained by the substitution of (30) into (13):

$$V_{KY}^{\psi} \approx -D/2\cos\psi\,\dot{\psi};\ V_{KX}^{\psi} \approx D/2\sin\psi\,\dot{\psi};\ V_{KZ}^{\psi} \approx V_{B1Z}^{\psi} \approx V_{B2Z}^{\psi} \approx 0.$$
$$V_{B1X}^{\psi} \approx V_{B2X}^{\psi} \approx -D/2\sin\psi\,\dot{\psi};\ V_{B1Y}^{\psi} \approx V_{B2Y}^{\psi} \approx -D/2\cos\psi\,\dot{\psi}; \tag{33}$$

The expressions (33) describe the horizontal rotation of the contact points around the hole axis with radius $D/2$ and angular velocity $\dot{\psi}$. Again, the reduction contact points B_1 and B_2 to a single point B opposite to K is obvious here.

The expression of velocities components for the *slip* motion, related to the peg self-rotational angle φ could be obtained by the substitution of (30) into (18):

$$V_{KY}^{\varphi} \approx -D/2cos\psi\,\dot{\varphi};\quad V_{KX}^{\varphi} \approx D/2\sin\psi\,\dot{\varphi};\quad V_{KZ}^{\varphi} \approx V_{B1Z}^{\varphi} \approx V_{B2Z}^{\varphi} \approx 0.$$
$$V_{B1X}^{\varphi} \approx V_{B2X}^{\varphi} \approx -D/2\cos\psi\,\dot{\varphi};\quad V_{B1Y}^{\varphi} \approx V_{B2Y}^{\varphi} \approx D/2\cos\psi\,\dot{\varphi}; \tag{34}$$

Expressions (34) could be interpret as the horizontal rotation of the contact points around the peg axis with radius $d/2 \approx D/2$. Due to small gap between the parts and small angle of misalignment, (33) and (34) become equivalent. Which mean that although mathematically slip and slide are still independent, physically they become indistinguishable, and could be considered as one.

Expressions (32–34) allow to obtain simplified formulae for (19) for the full velocities components:

$$V_{B1X} \approx V_{B2X} \approx -D/2\sin\psi\left(\dot{\psi} + \dot{\varphi}\right);\quad V_{B1Y} \approx V_{B2Y} \approx D/2\cos\psi\left(\dot{\psi} + \dot{\varphi}\right);\quad V_{KZ} \approx 0$$
$$V_{KX} \approx D/2\sin\psi\left(\dot{\psi} + \dot{\varphi}\right);\quad V_{KY} \approx -D/2\cos\psi\left(\dot{\psi} + \dot{\varphi}\right);\quad V_{B1Z} \approx V_{B2Z} \approx -D\dot{\gamma}. \tag{35}$$

From (35) it is easy to get the full absolute of velocities:

$$V_{B1}\approx V_{B2}\approx D/2\sqrt{\left(2\dot{\gamma}\right)^2+\left(\dot{\psi}+\dot{\varphi}\right)^2};\quad V_K=D/2\left(\dot{\psi}+\dot{\varphi}\right). \tag{36}$$

In (36) the same rotational components for the velocities at all points around the approximate common axis of the peg and the hole is obvious. The vertical component of the planar motion of the reduced points B_1 and B_2 is also clearly visible.

Now the expressions (30–36) could be substituted to DDE (28) to get the approximation of the small alignment angle. Here we assume that all the motions are ensured by the torque caused by the compensated pair of the forces. It would mean that the projections of the joint external forces to the axis are zero. We also assume the homogeneous rotation in all three degrees of freedom: $\dot{\gamma}=\text{const}, \dot{\varphi}=\text{const}, \dot{\psi}=\text{const}$. In order to get the values for the reaction forces only the Eqs. (28.4–28.6) will be in the focus of attention.

$$N_K(\cos\psi-f\sin\psi)+(N_{B1}+N_{B2})\left(-\cos\psi+\frac{f\sin\psi(\dot{\psi}+\dot{\varphi})}{\sqrt{(2\dot{\gamma})^2+(\dot{\psi}+\dot{\varphi})^2}}\right)=m\left[-D/2\cos\psi\dot{\gamma}^2+H\sin\psi\dot{\gamma}\dot{\psi}\right]; \tag{37.1}$$

$$N_K(\sin\psi+f\cos\psi)+(N_{B1}+N_{B2})\left(-\sin\psi-\frac{f\cos\psi(\dot{\psi}+\dot{\varphi})}{\sqrt{(2\dot{\gamma})^2+(\dot{\psi}+\dot{\varphi})^2}}\right)=m\left[-D/2\sin\psi\dot{\gamma}^2+H\cos\psi\dot{\gamma}\dot{\psi}\right]; \tag{37.2}$$

$$N_K\gamma_0+(N_{B1}+N_{B2})\frac{f2\dot{\gamma}}{\sqrt{(2\dot{\gamma})^2+(\dot{\psi}+\dot{\varphi})^2}}=m(-D/\gamma_0-H/2)\dot{\gamma}^2+mg. \tag{37.3}$$

To analyse the motion further, we notice that the most reasonable assumptions detail sizes are of the order of cm, of the gap—of the order of 0.1 mm, of the align speed – of the order of 1 1/s. With respect to these estimations, the acceleration of the free fall ~10m/s^2 has a much higher value. So it will be the most significant term at the right part of (37.3). As the last part of the simplification of (37), the direction of the axes X and Y are chosen without reduction of generality to fulfil $\cos\psi=1$. The expressions of (37) will turn to:

$$N_K-(N_{B1}+N_{B2})\approx -m\mathrm{D}/2\dot{\gamma}^2; \tag{38.1}$$

$$fN_K-f(N_{B1}+N_{B2})\frac{(\dot{\psi}+\dot{\varphi})}{\sqrt{(2\dot{\gamma})^2+(\dot{\psi}+\dot{\gamma})^2}}\approx -mH\dot{\gamma}\dot{\psi}; \tag{38.2}$$

$$N_K\gamma_0+(N_{B1}+N_{B2})\frac{f2\dot{\gamma}}{\sqrt{(2\dot{\gamma})^2+(\dot{\psi}+\dot{\varphi})^2}}\approx mg. \tag{38.3}$$

From (38) it could be deduced that although geometrically (i.e., from the left-hand side of the equations), slip and slide are indistinguishable, it is the mechanics (i.e., right-hand side) that makes them independent. Despite all the approximations, slip does not change the position of the mass center of the peg by the definition of slip, but slide does.

Deriving N_K from (38.1), and substituting it into (38.3) we could derive the expression for $(N_{B1}+N_{B2})$, and find N_K. We assumed here that the right-hand side of (38.1) is negligible with gravity force.

$$(N_{B1}+N_{B2})\approx N_K\approx\frac{mg}{\gamma_0+f\dfrac{2\dot{\gamma}}{\sqrt{(2\dot{\gamma})^2+(\dot{\psi}+\dot{\varphi})^2}}}. \tag{39}$$

Both γ_0 and f are small values, so the reaction forces at the moment of transition from three-point to two-point contacts are very high. The value for the forces could vary form $mg/(\gamma_0+f)$ to mg/γ_0. For the parameters assumed in the beginning of this subsection, the first value equals approximately 3.8 weights of the peg (i.e., mg) and is realized for a pure align with no slide and slip. The second value equals approximately 15.8 mg and is realized for high slide and slip rotational velocities, when the rotational velocity of the align becomes negligible.

3 Conclusions

A detailed kinematic analysis of compound motion of peg supported at the edge of vertically fixed hole was performed. In this analysis all three degrees of freedom in the course of alignment process were taken into account. The directions of interaction forces were identified at the peg and hole contact points.

Dynamic Differential Equations providing the most general description of a process of aligning cylindrical parts were written. They describe the mutual dependence between the motion of the parts during the three-point contact, the forces ensuring this motion and the reaction forces at the points of contact.

DDE enables to analyse all possible alternatives of vertical assembly, to determine interaction forces of parts at contact points, to find the required forces for the required motion, or to find the motion with given external forces.

As partial cases, the alignment motion with and without slip were compared. It was identified that the reaction forces during alignment are increased, and that slip could decrease the forces a bit. DDE were analysed for the small angles of alignment. It was established that near the transition into a two-point contact, the reaction forces are very high, and additional slide and slip makes them even higher.

The application of peg compound motion may help to select parameters and modes of assembly, optimize the reaction forces for the small gaps, use predictions to recognize the contact state.

References

1. Lefebvre T, Xiao J, Bruyninckx H, De Gersem G (2005) Active compliant motion: a survey. Adv Robot 19(5):479–499
2. Xu J, Hou Z, Liu Z and Qiao H (2019) Compare contact model-based control and contact model-free learning: a survey of robotic peg-in-hole assembly strategies arXiv, 1904.05240 https://arxiv.org/abs/1904.05240
3. Whitney DE (1982) Quasi-static assembly of compliantly supported rigid parts. J Dyn Syst Meas Control 104(1):65–77
4. Jasim IF, Plapper PW, Voos H (2017) Contact-state modelling in force-controlled robotic peg-in-hole assembly processes of flexible objects using optimised gaussian mixtures. Proc Inst Mech Eng B J Eng Manuf 231(8):1448–1463
5. Fei Y, Zhao X (2003) An assembly process modeling and analysis for robotic multiple peg-in-hole. J Intell Robot Syst 36(2):175–189
6. Xu J, Hou Z, Wang Q, Xu B, Zhang K, Chen K (2018) Feedback deep deterministic policy gradient with fuzzy reward for robotic multiple peg-in-hole assembly tasks. IEEE Trans Ind Inf:1–1
7. Tang T, Lin HC, Zhao Y, Chen W, Tomizuka M (2016) Autonomous alignment of peg and hole by force/torque measurement for robotic assembly. Automation Science and Engineering (CASE), 2016. IEEE International Conference, New Jersey, pp 162–167
8. Abu-Dakka F, Nemec B, Ude A (2012) Peg-in-hole using dynamic movement primitives. In: Proceedings of the RAAD, pp 143–149
9. Zhu Z, Hu H (2018) Robot learning from demonstration in robotic assembly: a survey. Robotics 7(2):17–17
10. Kyrarini M, Haseeb MA, Risti'c-Durrant D, Gräser A (2018) Robot learning of industrial faassembly task via human demonstrations. Auton Robot:1–19
11. Tang T, Lin HC, Zhao Y, Fan Y, Chen W, Tomizuka M (2016) Teach industrial robots peg-hole-insertion by human demonstration. In: Advanced Intelligent Mechatronics (AIM), 2016. IEEE International Conference, New Jersey, pp 488–494
12. Liljekrans D (2012) Investigating peg-in-hole strategies through teleoperation. Master's Thesis. University of Southern Denmark. http://citeseerx.ist.psu.edu/viewdoc/download?doi=10.1.1.727.7529&rep=rep1&type=pdf
13. Savarimuthu TR (2013) Analysis of human peg-in-hole executions in a robotic embodiment using uncertain grasps. In: Proceedings of the 9th International Workshop on Robot Motion and Control, pp 233–239. https://doi.org/10.1109/RoMoCo.2013.6614614
14. Sutton RS, Barto AG (2018) Reinforcement learning: an introduction MIT press
15. Inoue T, Magistris GD, Munawar A, Yokoya T, Tachibana R (2017) Deep reinforcement learning for high precision assembly tasks. 2017 IEEE/RSJ International Conference on Intelligent Robots and Systems (IROS), Canada, pp 819–825
16. Xu J, Hou Z, Wang W, Xu B, Zhang K, Chen K (2018) Feedback deep deterministic policy gradient with fuzzy reward for robotic multiple peg-in-hole assembly tasks. IEEE Trans Ind Inf:1–1
17. Thomas G, Chien M, Tamar A, Ojea JA, Abbeel P (2018) Learning robotic assembly from CAD. arXiv 1803.07635http://arxiv.org/abs/1803.07635
18. Su J, Qiao H, Liu C, Ou Z (2012) A new insertion strategy for a peg in an unfixed hole of the piston rod assembly. Int J Adv Manuf Technol 59:1211–1225. https://doi.org/10.1007/s00170-011-3569-y
19. Xia Y, Yin Y. Zhaoneng Chen Z (2006) Dynamic analysis for peg-in-hole assembly with contact deformation. Int J Adv Manuf Technol 30: 118–128. https://doi.org/10.1007/s00170-005-0047-4
20. Zamyatin VG(1972) Geometric conditions of the assemblability during automatic assembly of the cylindrical junctions with gap. (Геометрические условия собираемости при автоматической сборке цилиндрический соединений с зазором). Proceedings of higher educational institutions. Machine Building 12: 162–166
21. Kristal MG (2000) Estimation of the error of the relative positions of the conjugated surfaces during the automated assembly of cylindrical details. (Оценка погрешности относительного расположения сопрягаемых поверхностей при автоматической сборке цилиндрических деталей). Assem Mach Build Dev Build 6:20–23
22. Peeva II, Vipliemov VD (2009) Passive-active relative orientation in conditions of the automated assembly. (Пассивно-активное относительное ориентирование в условиях автоматической сборки). Assem Mach Build Dev Build 6:23–26
23. Simakov AL, Simakov AD (2009) Alignment of the stages of the orientation of the attaching detail during the motion on the searching trajectory. (Согласование этапов ориентации присоединяемой детали при движении по поисковой траектории). Assem Mach Build Dev Build 6:20–22
24. Kuznetsov SV, Simakov AL (2013) Phase portraits of the relative and angular alignment of the details during the automated alignment. (Фазовые портреты относительного и углового совмещения деталей при автоматической сборке). Assem Mach Build Dev Build 2:12–20
25. Holodkova AG (2004) Peculiarities of the automated executions of the cylindrical joints with small gap. (Особенности автоматического выполнения цилиндрических соединений с малым зазором). Assem Mach Build Dev Build 4:14–18
26. Ivanov AA (2009) Analytical conditions of the automated assembly. (Аналитические условия автоматической сборки). Assem Mach Build Dev Build 8:13–17
27. Chernyakhovskaya LB, Simakov DA (2012) Kinematics and dynamics of the process of the assembly of cylindrical details. (Кинематика и динамика процесса сборки цилиндрических деталей). Assem Mach Build Dev Build 1:27–42
28. Jarkov GE, Prilutskiy VA (2012) Selfadjustment of the positions of details during the assembly. (Саморегулирование положения детали при сборке). Assem Mach Build Dev Build 9:12–14
29. Jarkov GE (2014) Method of the assembly by the change of the position of mass center. (Метод сборки изменением положения центра тяжести). Assem Mach Build Dev Build 11:7–9
30. Bojkova LV, Vartanov MV, Zimina IN (2015) Mathematical model of the robotized assembly with use of adaptation and low-frequency oscilations. (Математическая модель роботизированной сборки с применением адаптации и низкочастотных колебаний). Assem Mach Build Dev Build 16:16–20
31. Ivanov AA (2013) Vibrational assembly systems. (Вибрационные сборочные системы). Assem Mach Building Dev Build 5:7–10
32. Bakšys B, Chadarovičius A, Pilkauskas K (2009) Experimental research of parts vibratory alignment with remote center compliance device. J Vibroeng 11(2):226–232

33. Bojkova LV, Vartanov MV, Martynovich NA (2013) Mathematical model of dynamics of the conjunction of the details with use of an industrial robot and a vibrational device (Математическая модель динамики сопряжения деталей с применением промышленного робота и вибрационного устройства). Assem Mach Build Dev Build 1:12–15
34. Kristal MG, Chuvilin IA (2008) Investigation of the dynamics of vibrational conjunction with the lower support of the edge of the enclosed detail. (Исследование динамики вибрационного сопряжения с нижней опорой торца охватываемой детали). Assem Mach Build Dev Build 4:13–17
35. Kristal MG, Chuvilin IA (2008) Model of the dynamics of rotational assembly of cylindrical details. (Модель динамики ротационной сборки цилиндрических деталей.). Assem Mach Build Dev Build 8:12–15
36. Kremleva NG, Bezrukova TB (2015) Investigation of the process of automated rotational assembly of cylindrical details. (Исследование процесса автоматической ротационной сборки цилиндрических деталей). Assem Mach Build Dev Build 6:29–32
37. Bruyninckx H, Demey S, Dutre S, De Schutter J (1995) Kinematic models for model based compliant motion in the presence of uncertainty. Int J Robot Res 14(5):465–482. https://doi.org/10.1177/027836499501400505
38. Bruyninckx H, Dutre S, De Schutter J (1995) Peg-on-hole: a model based solution to peg and hole alignment. In: Proceedings of the IEEE International Conferenceon Robotics and Automation, pp 1919–1924. https://doi.org/10.1109/ROBOT.1995.525545
39. Chernyakhovskaya LB, Simakov DA (2017) Peg-on-hole: fundamental principles of motion of a peg leaning on a horizontal hole edge. Adv Sci Technol Res J 11(4):49–59. https://doi.org/10.12913/22998624/77036